

Silicone-Based Lubricant-Infused Slippery Coating Covalently Bound to Aluminum Substrates for Underwater Applications

Lucia H. Prado, David Böhringer, Anca Mazare, Lamborghini Sotelo, George Sarau, Silke Christiansen, Ben Fabry, Patrik Schmuki, Sannakaisa Virtanen, Wolfgang H. Goldmann,* and Alexander B. Tesler*



Cite This: <https://doi.org/10.1021/acsami.3c04508>



Read Online

ACCESS |

Metrics & More

Article Recommendations

Supporting Information

ABSTRACT: Wetting of solid surfaces is crucial for biological and industrial processes but is also associated with several harmful phenomena such as biofouling and corrosion that limit the effectiveness of various technologies in aquatic environments. Despite extensive research, these challenges remain critical today. Recently, we have developed a facile UV-grafting technique to covalently attach silicone-based coatings to solid substrates. In this study, the grafting process was evaluated as a function of UV exposure time on aluminum substrates. While short-time exposure to UV light results in the formation of lubricant-infused slippery surfaces (LISS), a flat, nonporous variant of slippery liquid-infused porous surfaces, longer exposure leads to the formation of semi-rigid cross-linked polydimethylsiloxane (PDMS) coatings, both covalently bound to the substrate. These coatings were exposed to aquatic media to evaluate their resistance to corrosion and biofouling. While the UV-grafted cross-linked PDMS coating effectively inhibits aluminum corrosion in aquatic environments and allows organisms to grow on the surface, the LISS coating demonstrates improved corrosion resistance but inhibits biofilm adhesion. The synergy between facile and low-cost fabrication, rapid binding kinetics, eco-friendliness, and nontoxicity of the applied materials to aquatic life combined with excellent wetting-repellent characteristics make this technology applicable for implementation in aquatic environments.

KEYWORDS: lubricant-infused slippery surfaces, polydimethylsiloxane, corrosion resistance, anti-biofouling, biofilms, UV-grafting, cross-linking



1. INTRODUCTION

The oceans that cover ~70% of the surface of our planet are in constant motion due to wind, the moon, and the planet's rotation, temperature, and salinity differences.¹ While such endless movements provide food and oxygen to aquatic life and move ships across the ocean,² they are also regarded as a green, renewable, and reliable source of energy around the world. However, the potential of the ocean as one of the greatest sources of energy is under-explored compared to other green alternatives.³ This is because the aquatic environment is extremely challenging due to (i) the high concentration of ions such as chlorine, which leads to increased corrosion of metals, and (ii) the accumulation of aquatic organisms on solid surfaces, i.e., biofouling, which degrades the desired functionality of devices.

Among the available engineering materials, aluminum (Al) is one of the most widely used structural metals in marine applications due to its lightweight, high strength, good corrosion resistance, easy recyclability, extrudability, and weldability for design flexibility. Today, it is used in fast ferries, wave-piercing catamarans, cruise ships, as well as offshore oil drilling rigs, deep submersible vessels, and helicopter landing pads, to name but a few,⁴ in its pure form or as an alloy to adjust the mechanical and corrosion

properties.^{5,6} It is common knowledge that Al is susceptible to corrosion. Under mild conditions (e.g., the near-neutral pH range of many aqueous solutions), Al exhibits stable passivity and, hence, very low corrosion rates.^{7,8} However, under more aggressive conditions, Al can corrode severely.⁹ The most common type of corrosion is pitting, which occurs in the presence of chloride ions.¹⁰ In addition to direct corrosion-related structural failures of constructions, this results in the release of Al ions into the marine environment, which can be toxic to aquatic life.¹¹

However, it is well known that Al is neither required in biological systems nor involved in any essential biological processes.¹² Nevertheless, all living organisms today contain some aluminum due to its abundance in the Earth's crust. On the contrary, there are known biological effects of Al, most of which are negative.¹³ The toxicity of Al is closely related to pH, as the metal is soluble and biologically available in acidic (pH <

Received: March 29, 2023

Accepted: May 15, 2023

5.5) soils and waters but relatively harmless in neutral conditions (pH = 5.5–7.5). Forest dieback and impaired reproduction of aquatic invertebrates, fish, and amphibians have been directly linked to Al toxicity.¹¹

Another issue to consider in aquatic applications is biofouling, which is the undesired colonization and accumulation of aquatic organisms on submerged surfaces.¹⁴ Biofouling is a multistep process initiated by the formation of a “conditioning layer” of microfoulers, which are bacteria, diatoms, and/or microalgae that promote the formation of biofilm matrix upon which multicellular micro- and macrofoulers develop.¹⁵ For centuries, it has been common practice to apply anti-biofouling coatings containing toxic biocidal chemicals to prevent biofouling by locally killing or slowing down their growth.^{16,17} Such anti-biofouling coatings typically contained active biocidal chemicals based on As, Sn, Cu, and Zn, among others.^{17–19} Over time, the environmental impact of these compounds became apparent on aquatic life, and in particular on nontarget fouling organisms, which finally led to their banning in 2008, opening up a new era in the development of nontoxic anti-biofouling coatings.²⁰ In particular, the focus is on reducing the attachment or increasing the release of biological foulants from the surface by tailoring the surface properties of the material, such as energy, roughness, wettability, and chemistry. In this regard, superhydrophobic surfaces have been studied for many years as a vital solution for anti-biofouling surfaces.²¹ The trapped air layer, so-called plastron, formed on a superhydrophobic surface reduces the contact between the biomaterial-containing fluid and the substrate. However, to date, the plastron on engineered superhydrophobic surfaces has been shown to be metastable, making such surfaces unsuitable for long-term immersion.²² Furthermore, the increased surface roughness after plastron loss triggers surface coverage by fouling organisms and also provides a larger surface area to accelerate corrosion. Therefore, in 2011, a new type of coating called slippery liquid-infused porous surfaces (SLIPS) was introduced.²³ Inspired by the *Nepenthes* pitcher plant, the surface chemistry and roughness were tailored to immobilize a liquid layer on the rough solid surface, thereby introducing an additional liquid–liquid interface that separates the solid substrate from direct contact with an aggressive and fouling liquid.²⁴ By controlling the composition and viscosity of the lubricant, a wide variety of liquids can be repelled.^{25–34} However, there are several drawbacks associated with the SLIPS technology: (i) the requirement for rough, porous structuring of the substrate surface, which weakens the mechanical robustness, and (ii) the multistep preparation processes.²³

Recently, we developed a one-pot process to form a nontoxic lubricant-infused slippery surface (LISS) coating on smooth surfaces based on the UV-grafting of polydimethylsiloxane (PDMS or silicone oil).³⁵ A layer of PDMS molecules is covalently grafted to the solid surface by selective dissociation of the Si–CH₃ terminal bond, lowering the surface energy of the substrate and matching it to the surface tension of the nongrafted, i.e., residual PDMS used as the infusing lubricant. PDMS is commercially available, inexpensive, and nontoxic to aquatic environments, providing an optimal solution compared to fluorinated compounds. Previously, we demonstrated that the UV-grafted LISS coating prepared on austenitic stainless steel prevented the adhesion of aquatic organisms even when severely damaged.³⁶

In this study, we fabricated a UV-grafted PDMS coating on aluminum to simultaneously investigate the resistance of the UV-grafted PDMS coatings to corrosion and biofouling in aquatic environments. Corrosion of metallic substrates can deteriorate the stability of the infused lubricant, increase its depletion, and ultimately lead to coating failure. This is because metal oxides have a high surface energy,³⁷ which makes them significantly less attractive for wetting by low surface tension liquids such as lubricants, which is contrary to the basic requirement for liquid-infused surfaces.²³ First, the LISS coating was fabricated according to our previously reported process.^{35,36} Then, the UV exposure time was extended to achieve a cross-linked PDMS (CL-PDMS) coating. In both cases, PDMS is covalently grafted onto the substrate. The corrosion protection of the UV-grafted coating was investigated by potentiodynamic polarization curves measured in an aqueous electrolyte containing 3.5 wt % NaCl and by long-term immersion in freshwater and seawater media. Finally, the UV-grafted and bare aluminum samples were exposed to aquatic organisms such as freshwater algae and seawater diatoms, the latter known as early colonizers.^{38,39} We show that the LISS coating is effective in preventing biofouling adhesion, while the CL-PDMS is superior in corrosion protection of Al in aquatic environments.

2. EXPERIMENTAL SECTION

2.1. Materials. Aluminum 1000-grade sheets of 1 mm thickness (99.5% Al) were purchased from Advent Research Materials, UK. Polydimethylsiloxane (PDMS, silicone oil) with a viscosity of 500 cSt ($M_w = 17.3$ kDa), ethanol, acetone, and toluene were purchased from Carl Roth, Germany, and used as received. Deionized water with a specific resistance of 18.2 M Ω /cm was used in all experiments.

2.2. Fabrication of UV-Grafted PDMS Coatings. Aluminum sheets were cut into 25 × 25 × 1 mm size specimens and used as substrates. The substrates were first ground with a SiC abrasive paper up to 1200 grit. The substrates were then ultrasonically degreased in acetone and ethanol for 10 min and then dried under a stream of N₂. These samples were placed horizontally in a glass Petri dish under a quartz cover and covered with approx. 20 μ L cm⁻² of silicone oil (PDMS) pipetted to cover the entire sample surface. The samples were then illuminated using a medium-pressure ultraviolet (UV) (Hg) lamp at 1 kW (UVAPRINT HPV, Höppler AG, Germany) at a working distance of 30 cm. The emission maxima of this type of lamp are in the UV range, i.e., $\lambda = 320$ and 365 nm. A power density at the working distance of ~ 100 mW cm⁻² at $\lambda = 320$ nm was measured using a Newport 1830-C optical power meter equipped with an 818-UV/DB optical power detector and a 1% Newport ND filter. The PDMS-coated substrates were illuminated for either 30 or 180 min to form the LISS or CL-PDMS coating, respectively.

2.3. Measurement of Cross-Linking Percentage. To estimate the portion of cross-linking, the ASTM D2765-16 standard procedure was applied. Here, the 50 × 50 mm CL-PDMS on Al substrates were soaked in toluene for 24 h at room temperature to dissolve unbound silicone oil. Then, the samples were dried under vacuum for 12 h at room temperature, followed by heat treatment at 100 °C in a vacuum oven for 4 h. The cross-linked UV-grafted samples were weighed before and after the soaking/dissolution/drying process, and the percentage of cross-linking was obtained as follows: $G = M_2/M_1 \times 100\%$, where G is the cross-linking percentage, M_1 and M_2 are the masses of the samples before and after the soaking/dissolving/drying process.

2.4. Contact Angle and Hysteresis Measurements. Apparent water contact angle (WCA) measurements were carried out using a DSA100 contact angle goniometer (KRÜSS, Germany). A small drop was deposited on the surface, and the volume was increased to ~ 10 μ L, and then the WCA was measured using the Laplace–Young model for a sessile droplet. For contact angle hysteresis (CAH), the

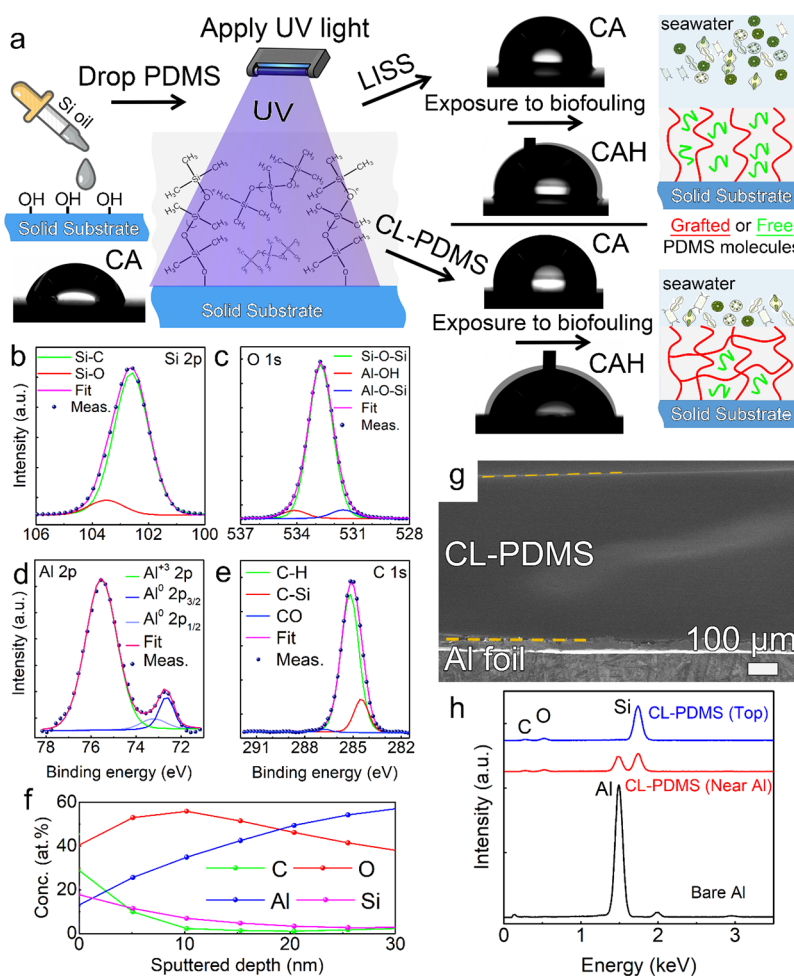


Figure 1. (a) Schematic representation of the silicone oil UV-grafting process to convert Al surfaces into either LISS or CL-PDMS coatings, both covalently bound to the substrate. (b–e) High-resolution XPS spectra of (b) Si 2p, (c) O 1s, (d) Al 2p, and (e) C 1s. (f) XPS depth profile of Si, C, O, and Al, UV-grafted PDMS on polished Al substrates. (g) Cross-sectional SEM image of the CL-PDMS layer prepared on 200 μm thick Al foil. Air–PDMS and PDMS–aluminum foil interfaces are highlighted by orange dashed lines. (h) EDX analysis of bare and CL-PDMS (measured at the top and near the Al substrate) UV-grafted on polished Al substrates.

drop volume of 20 μL was increased and decreased at a rate of 0.05 $\mu\text{L s}^{-1}$ under video recording. Fitting was performed using the Ellipse method (Tangent-1) using the KRUSS Drop Shape Analysis software. It should be noted that the calculated values obtained by the Ellipse fitting algorithm for CAH are lower than those calculated by the Laplace–Young fitting algorithm for the apparent contact angle; therefore, only the difference between the advancing and receding CAs should be considered as a CAH (not the absolute calculated value). All values given in the text were averaged from at least three independent measurements.

2.5. Attenuated Total Reflectance Fourier Transform Infrared Spectroscopy Measurements. A Jasco FT/IR-4700 spectrometer (Tokyo, Japan), equipped with a Jasco ATR-PRO ONE attachment, a single-bounce ATR with a monolithic diamond, was used. Attenuated total reflectance Fourier transform infrared (ATR-FTIR) spectra were recorded in the range of 6000–220 cm^{-1} with 64 scans and a resolution of 1 cm^{-1} . Air was measured immediately before the sample and used as a background. In the case of pure silicone oil, a volume of 10 μL was dropped directly onto the diamond crystal.

2.6. Raman Spectroscopy Measurements. A LabRam HR800 spectrometer from Horiba was used in a backscattering geometry under ambient room temperature conditions. An excitation wavelength of 532 nm was used paired with a 50x long working distance objective (NA 0.55, Leica), a grating of 300 lines mm^{-1} , and a laser power of 6 mW to avoid material damage and molecular changes.

Power dependence tests were performed to explore the optimal measurement conditions prior to data acquisition. A set of 3 maps, each consisting of 6561 measurement points, was obtained on both planar PDMS and CL-PDMS samples, resulting in statistically significant mean Raman spectra.

2.7. Potentiodynamic Polarization and Long-Term Immersion Tests. Corrosion experiments were performed in a 3.5 wt % NaCl aqueous electrolyte with a three-electrode configuration, using the sample as the working electrode, a platinum electrode as the counter electrode, and a HydroFlex hydrogen reference electrode. The samples, used for potentiodynamic polarization, were coated with a Bonderite S-MA 527 HT resin (Henkel AG & Co, Germany) exposing an area of $\sim 1.5 \text{ cm}^2$, which was subsequently coated with either the LISS or CL-PDMS. The sample, coated with a Bonderite S-MA 527 HT resin, was in contact with the electrolyte through a circular O-ring sealed opening in the cell wall, contacting only the resin and not with the PDMS-coated surface, exposing a circular area of 20 mm in diameter. For each sample, open-circuit potential (OCP) measurements (Zahner Zennium Electrochemical Workstation) were performed until a stable OCP value was reached, followed by potentiodynamic polarization from -100 mV vs the OCP until 0.3 V vs the reference electrode at a scanning rate of 1 mV s^{-1} . Long-term corrosion resistance measurements were performed by immersing bare, LISS, and CL-PDMS Al substrates in fresh and artificial seawater media in a Petri dish in an ambient atmosphere. Digital and bright-field optical microscopy images were taken after 85 and 143 days of

immersion, and the samples were returned to aquatic media for further evaluation of the extent of corrosion resistance.

2.8. Freshwater Green Algae Laboratory Assay. The stock solution of the green algae *Chlamydomonas reinhardtii* (*C. reinhardtii*, CCAP #11/32B) was purchased from the Scottish Association for Marine Science (CCAP) and used as a model organism to study biofilm adhesion on LISS and CL-PDMS surfaces. *C. reinhardtii* was grown in a 3N-BBM+V medium solution (CCAP FA3N-C) under nonaxenic conditions. The stock culture solution was placed under a fluorescent daylight lamp (Philips TL5HO) fixture and grown continuously with 16/8 h on/off light cycles at room temperature (18–20 °C) under rocking conditions.

2.9. Seawater Diatom Laboratory Assay. The seawater diatom of the type *Odontella aurita* (*O. aurita*, CCAP, #1054/1) purchased from the Scottish Association for Marine Science (CCAP) was used as a model organism to study biofilm adhesion on LISS and control samples. *O. aurita* was grown in an f/2 + Si seawater medium (CCAP, Guillard's medium for diatoms) under nonaxenic conditions. Stock culture solutions were placed under a fluorescent light (Philips TL5HO) fixture at room temperature (18–20 °C) and grown continuously with 16/8 h on/off light cycles under rocking conditions. Seawater was prepared as described in the literature.⁴⁰

2.10. Morphology and Physicochemical Characterization. A field-emission scanning electron microscope (Hitachi FE-SEM S4800) equipped with an energy-dispersive X-ray spectrometer (Genesis, Oxford Instruments) was used for morphological characterization. The composition and the chemical state of the films were characterized using X-ray photoelectron spectroscopy (XPS, PHI 5600, US), and the spectra were shifted according to the Al 2p metal peak at 72.7 eV, and the peaks were fitted using a PHI MultiPak software (symmetrical peak shape, except for Al metal). Depth profiling was carried out using the instrument's Ar⁺ sputter source operated at 3 kV and 15 nA, rastered over a 3 × 3 mm² area at a sputtering angle of 45° to the surface. Sputtering steps of 1 min were repeated until the Al substrate was reached. The atomic composition was determined between successive sputtering intervals by evaluating the photoelectron peak area using a PHI MultiPak processing software. The sputtering rate was calibrated using commercial Si/SiO₂ wafers (3 inch Si(100) p-type with 100 nm SiO₂, μChemicals, Germany) and was found to be 2 nm min⁻¹.

2.11. Biofouling Experiments. Bare polished, LISS, and CL-PDMS Al samples were placed horizontally in a 10 cm diameter polystyrene Petri dish with three samples of 2.5 × 2.5 cm each per dish. Freshwater green algae and seawater diatoms were used to examine biofilm retention on all surfaces. The stock solution was diluted 1:5 with the appropriate growth medium. The surface of each sample was then covered with ~80 mL of culture medium (~1 cm thick above the substrate surface). All the samples were incubated at ~20–23 °C (room temperature) for 8 days with 16/8 h on/off illumination to allow for proper biofilm growth. After 8 days, the samples were photographed and then pulled out of the culture medium at a controlled rate of 0.5 mm s⁻¹ using a dip coater (RDC15, Bungard, Germany). Treated substrates were photographed immediately after removal from the culture to avoid biofilm retraction. The images were then analyzed using ImageJ to assess the residual biofilm coverage after the air–water interface transition. Triplicates were used for all biofouling experiments. In addition, images were captured by confocal microscopy (Leica, Wetzlar, Germany), bright-field optical microscopy (Nikon, Japan), and SEM (Hitachi, Japan).

2.12. Evaluation of the Surface Coverage by Fluorescence Confocal Microscopy. Algae and diatoms on the material surface were imaged using an upright laser-scanning confocal microscope (SPS, Leica, Wetzlar) equipped with a 10× objective (PL FLUOTAR, Leica, Wetzlar). For each material condition, the auto-fluorescence signal of algae or diatoms was recorded at 9–10 random surface positions (area of 590 × 590 μm with a voxel size of 0.6 μm per pixel). For each position, the area covered by algae and diatoms was segmented based on a uniform intensity threshold. The fraction of the area covered was then determined as the area covered by algae/diatoms divided by the total area.

3. RESULTS AND DISCUSSION

Figure 1a shows a schematic representation of the UV-grafting process of PDMS (i.e., silicone oil) used to convert 1000-grade Al surfaces into either LISS³⁵ or CL-PDMS coatings. Prior to UV-grafting, the substrates were ground to ensure the same surface roughness for all samples, and particularly for corrosion characterization, although the coating can be applied equally well to polished or rough surfaces regardless of their roughness characteristics. The formation process is simple, inexpensive, and easily scalable. The samples were placed horizontally in a glass Petri dish, and then, droplets of trimethylsilyloxy-terminated silicone oil (PDMS) were added to spread over the entire substrate surface. In this study, PDMS with a kinematic viscosity of 500 cSt ($M_w = 17.3$ kDa) was used. The setup was then illuminated with a medium-pressure mercury UV lamp at different times.

The typical spectrum of a light source is presented in Figure S1, Supporting Information. As shown, the most intense peaks in the UVA region correspond to $\lambda = 320$ and 365 nm. As we have previously shown, the 321 nm wavelength is the minimum required to dissociate the trimethylsilyl bonds of the PDMS terminal groups.³⁵ Other bonds, such as Si–O or even the backbone Si–CH₃, require higher energy photons, i.e., a lower wavelength, to ensure that there is a higher probability of preferentially dissociating the Si–CH₃ terminal bonds when using this source of UV irradiation. The UV-grafting process was previously tested on various metals and oxides, while the LISS samples were thoroughly washed in toluene to dissolve the remaining, nongrafted silicone oil, leaving only covalently bound PDMS molecules. It was shown that the surface was completely and homogeneously covered with covalently bound PDMS molecules.³⁵

To verify covalent bonding of PDMS molecules to Al substrates, a water contact angle (WCA) and X-ray photoelectron spectroscopy (XPS) were applied. Bare Al substrates are hydrophilic and exhibit a WCA of $74.0^\circ \pm 0.2^\circ$. Note that Al is considered a high surface energy material with a low WCA due to the formation of a native oxide layer.⁴¹ Here, such a relatively high WCA is due to hydrophobic contaminants, well in agreement with the literature,^{41,42} while the high-resolution XPS measurements support the adventitious carbon signature typical of airborne contamination (Figure S2, Supporting Information).⁴³ To form the LISS coating, Al samples were exposed to UV light for 30 min. The UV light partially dissociates silicone oil and covalently grafts it to the substrate, while the remaining nondissociated PDMS molecules are considered to be an infusing lubricant. The stability of LISS is ensured by matching the surface tension of the residual silicone oil with the surface energy of Al, which is composed of the same but covalently grafted PDMS molecules.²³ The LISS Al samples show a WCA and CA hysteresis (CAH) of $100.9^\circ \pm 3.9^\circ$ and $0.9^\circ \pm 0.5^\circ$, respectively (Figure 1a, top inset images), due to the liquid nature of the infused lubricant, i.e., the formation of the atomically smooth liquid surface typical for SLIPS/LISS.^{23,24,44}

To investigate the chemical composition and surface coverage of the UV-grafted PDMS layer on Al substrates, angle-resolved XPS analysis was performed at incident angles of 15°, 45°, and 75°, i.e., the detection depth changes due to the sample tilt angle. Silicone oil was UV-grafted to polished Al substrates, and the remaining oil was dissolved in toluene. The typical XPS survey spectra of these samples are shown in

Figure S3, Supporting Information, and the high-resolution XPS spectra are shown in Figure 1b–e. Bare Al was measured as a reference, showing Al, O, and C peaks (Figure S3a, Supporting Information). When UV-grafted, the survey XPS spectra consist mainly of Si, O, and C peaks associated with PDMS, while the Al 2p peak originating from the substrate is barely noticeable (Figure S3b, Supporting Information). The high-resolution Si 2p XPS spectrum consists of a single peak with a binding energy of 102.64 eV, which was deconvoluted into two components at 102.61 and 103.51 eV corresponding to Si–C and Si–O bonds, respectively (Figure 1b).⁴⁵ The O 1s spectra with the peak centered at 532.80 eV consist of three components: at 532.73 eV corresponding to the Si–O–Si bond (89.8%)⁴⁶ and at 531.53 and 534.13 eV corresponding to the Al–O–Si (5.3%) and Al–OH (4.9%) bonds, respectively (Figure 1c).^{47,48} When measured at an angle of 75°, the components corresponding to the substrate, Al–O–Si and Al–OH, increase slightly to 13.3 and 7.0%, respectively (Figure S4, Supporting Information). The high-resolution XPS peak of Al 2p was clearly observed at 45° and 75° but almost disappears at 15°, confirming that the PDMS-grafted layer covers the substrate entirely (Figure S5, Supporting Information). When measured at 45° and 75°, two peaks were observed at 72.70 and 75.55 eV, corresponding to metallic Al and its oxide (in the case of metallic Al, the peaks are asymmetric and the splitting of the 2p peak is evident with a spin separation of 0.44 eV, while the oxide has a symmetrical peak and the splitting can typically be ignored),^{49,50} respectively (Figures 1d and S5, Supporting Information).⁴⁸ The C 1s spectra show a single peak at 285.10 eV, which is associated with Si–C bonds (284.49 eV, 16.5%) and C–H bonds (285.19 eV, 82.5%) in PDMS, as well as small amounts of CO bonds (286.74 eV, 0.9%) (Figure 1e).⁵¹ The XPS sputter profiles of the UV-grafted PDMS on Al substrates demonstrate the thickness of the grafted layer to be ~10 nm, which is in good agreement with our previous results obtained on Si wafers (Figure 1f).³⁵

However, when the Al samples with silicone oil were exposed to UV irradiation for a longer time, i.e., 180 min, cross-linkage of PDMS was obtained. In this case, the coating appears as a thin semi-rigid layer in contrast to its liquid-like LISS counterparts (Figure 1g). The thickness of the CL-PDMS layer varies from tens to hundreds of microns as a function of the initial silicone oil volume dispersed (Figure S6, Supporting Information). The UV-grafted CL-PDMS layer has a CA and CAH of $98.7^\circ \pm 4.2^\circ$ and $8.6^\circ \pm 4.8^\circ$, respectively (Figure 1a, bottom inset images).

Attenuated total reflectance Fourier-transform infrared (ATR-FTIR) and Raman spectroscopy analyses were performed on polished Al, plain PDMS, LISS, and CL-PDMS to study the time dependence of the UV-grafting process on Al. The FTIR spectra in the wave number range of 250–4000 cm^{-1} are shown in Figure 2a. The peaks at 1258, 1065, 1011, and 788 cm^{-1} are the fingerprint for silicone oil.⁵² The two PDMS peaks at 1258 and 788 cm^{-1} are due to CH_3 deformation and CH_3 rocking in Si– CH_3 , respectively, and the two adjacent peaks at 1065 and 1011 cm^{-1} are due to Si–O–Si asymmetric deformation (Figure 2b). The peaks at 856 and 900 cm^{-1} in the CL-PDMS spectrum can be assigned to Si–O–Al bonds (Figure 2b, blue spectrum).⁵³ Figure 2c shows the symmetric and asymmetric CH_3 stretching peaks at 2962 and 2906 cm^{-1} , respectively.⁵⁴ A reduction in the peak intensity at 2962 cm^{-1} and a shift to 2963 cm^{-1} were observed

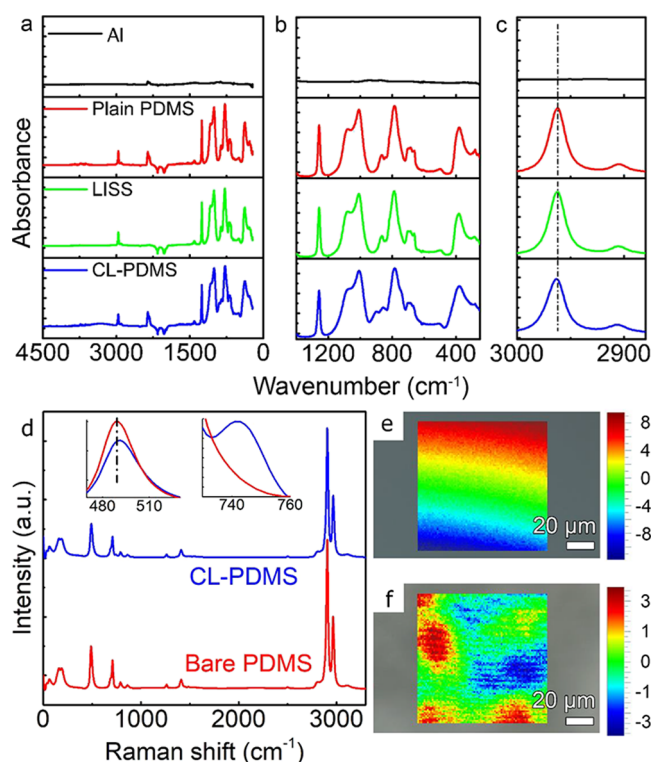


Figure 2. ATR-FTIR spectra in the wave number range of (a) 4500–250 cm^{-1} , (b) 1400–250 cm^{-1} , and (c) 3000–2880 cm^{-1} of the polished Al (black lines), plain PDMS (red lines), LISS (green lines), and CL-PDMS (blue lines) samples. (d) Mean Raman spectra and corresponding images of (e) plain and (f) UV-grafted CL-PDMS. The color bar in (e) and (f) indicates the percentage area change under the Si–O–Si peak.

in CL-PDMS. Such a shift of the methylene vibrations is generally believed to reflect an increase in the intermolecular interactions, improved long-range order, and, consequently, crystallinity of the PDMS layer.^{55,56}

Raman spectroscopy shows a typical spectrum of plain silicone oil with the repeating unit of $(\text{Si}(\text{CH}_3)_2\text{O})$ (Figure 2d). The intense peaks at 2965 and 2906 cm^{-1} in plain silicone oil correspond to the stretching modes of the CH_3 group, 1411 cm^{-1} (CH_3 asymmetric bending), 1260 cm^{-1} (CH_3 symmetric bending), and 862 (CH_3 symmetric rocking), 788 (CH_3 asymmetric rocking and Si–C asymmetric stretching), and 708 cm^{-1} (Si–C symmetric stretching) modes.⁵⁷ The peak at 688 cm^{-1} is assigned to the Si– CH_3 symmetric rocking mode, and the peak at 489 cm^{-1} corresponds to the Si–O–Si stretching mode.⁵⁸ Upon cross-linking, the Si–O–Si peak shifts to 491 cm^{-1} , and the faint peak at 742 cm^{-1} appears (Figure 2d). While the Si–O–Si peak shift to higher wavenumbers indicates the increase in hardening/crystallinity of the CL-PDMS, the peak at 742 cm^{-1} was typically observed in the thermally cured CL-PDMS elastomers.⁵⁹ The color maps in Figure 2e,f, superimposed on the optical images, show the area under the Si–O–Si peak, indicating only slight spatial differences in the thickness of the films. As can be seen, the percentage change calculated from the average of the entire map is smaller for the CL-PDMS as compared to the unlinked one. The latter can be attributed to the different sample preparation, i.e., the plain PDMS was dropped into an Al well, resulting in a drop-like thickness pattern after drying, while CL-PDMS forms a more uniform thick film under UV

illumination on a flat Al substrate. Finally, the standard ASTM D2765-16 procedure was used to estimate the degree of cross-linking. According to the calculations, the degree of cross-linking of UV-grafted samples exposed to UV irradiation for 180 min was $\sim 98\%$, while the CL-PDMS layer was barely swollen in toluene. The ATR-FTIR, Raman, and percentage cross-linking measurements indicate that with prolonged UV irradiation, there is a probability of dissociation of more than one trimethylsilyl bond to form a gel-like CL-PDMS coating.

As a next step, LISS and CL-PDMS coatings on Al were investigated for their resistance to wetting-related phenomena such as corrosion and biofouling in aqueous environments. As previously described, Al is a non-biocompatible material that is toxic to aquatic life.¹¹ Therefore, in addition to direct corrosion-related structural failure of metallic components, it is essential to protect Al from contact with a corrosive environment. Figure 3a shows potentiodynamic polarization

compared to the bare Al surface. However, no localized corrosion was observed on the surface of the LISS samples (Figure 3d). This is explained by a corrosion attack at the interface between the protective lacquer and the LISS coating, where crevice corrosion occurred (Figure S7, Supporting Information). When the potentiodynamic polarization was applied to the CL-PDMS coating, only noise was obtained and no current signal in response to polarization could be measured (Figure 3a, red spectrum, and 3e). This is due to the inability of the corrosive electrolyte to penetrate the cross-linked layer, as well as the covalent bonding of the PDMS to the Al substrate, making electrochemical measurements impossible. Such complete isolation of the material surface from an aggressive environment gains the system superior corrosion resistance.

Nevertheless, it has been shown previously that water can infiltrate PDMS.⁶¹ To investigate the long-term stability and corrosion protection of PDMS-based coatings, bare, LISS, and CL-PDMS were immersed in freshwater and seawater media for several months (Figures 3f and S8, Supporting Information). As shown, bare Al samples corrode severely in both freshwater and seawater media used to grow aquatic organisms (mimicking the freshwater and seawater composition) (see Tables S1 and S2 for chemical composition, Supporting Information). In the case of LISS and CL-PDMS, no corrosion was observed after 85 and 143 days. Note that this set of samples is still immersed in aquatic media, while the full period of corrosion protection will be published elsewhere.

One of the most challenging phenomena associated with the wetting of solid surfaces in aquatic environments is the formation of biofilms or biofouling. Biofilm formation is a complex, multistep process involving a wide variety of microorganisms. Once a solid is immersed in water, it adsorbs glycoprotein organic materials, forming a "conditioning film" within minutes. Bacteria, unicellular algae, and cyanobacteria (blue-green algae) are typically the next species to appear on the material, colonizing the material surface within hours.⁶² Species such as freshwater algae are critical to maintaining a healthy aquatic ecosystem as they increase the availability of dissolved oxygen for the organisms below, while the negative effects of Al on algae have been demonstrated.¹³ Here, green algae of the species *Chlamydomonas reinhardtii*, a motile alga that moves freely in the aquatic environment, were used as a freshwater model organism to study the growth and adhesion of algal biofilms on bare, CL-PDMS, and LISS-coated Al (Figure 4). Such green algal biofilms, grown on slippery lubricant-infused surfaces, have been shown to be remarkable indicators of the effectiveness of the liquid-infused layer.^{24,35,36,63,64} Here, treated and control samples were immersed in freshwater growth media with green algae for 8 days under a 16/8 h on/off illumination cycle, and the results are summarized in Figure 4a–d. Over the growth period, there was a significant increase in the algal density of LISS and CL-PDMS samples with no evidence of substrate-related growth reduction or mortality, indicating the nontoxic nature of the coating.

The surface coverage of green algae was obtained from digital and confocal fluorescence microscopy images. As shown in Figure 4a–c, freshwater green algae grow uniformly in Petri dishes. However, the biofilms formed on the treated and control samples show significantly different affinity to the substrates. When the bare samples were pulled through a water–air interface, algal biofilms were firmly attached to Al

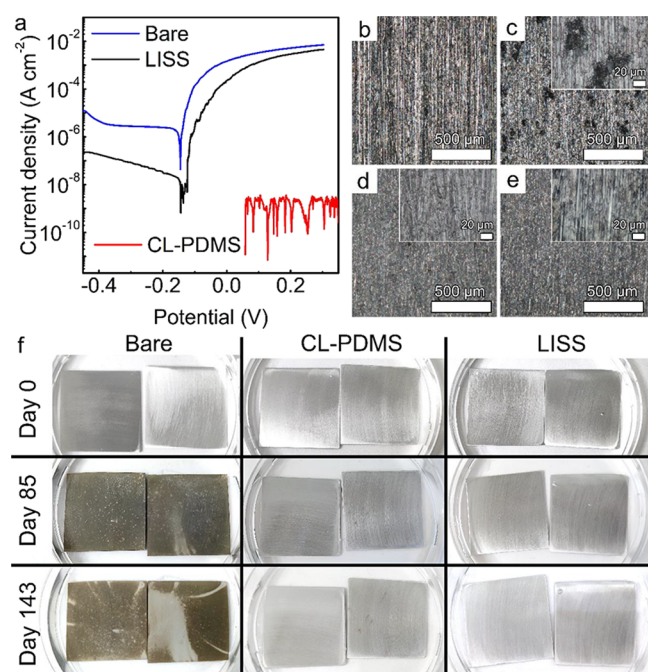


Figure 3. (a) Potentiodynamic polarization curves and (b–e) bright-field optical microscopy images of the ground bare aluminum surface before potentiodynamic polarization (b) and after potentiodynamic polarization of bare (c), LISS (d), and covalently bound CL-PDMS (e), measured in a 3.5 wt % NaCl aqueous electrolyte. (f) Digital images of bare, CL, and LISS covalently bound PDMS prepared on aluminum before (day 0) and after 85 and 143 days of submersion in artificial seawater.

curves measured in an aqueous electrolyte containing 3.5 wt % NaCl, the standard concentration used to simulate the seawater chloride concentration. Optical microscopy images show the original surface after the grinding and cleaning steps with micron-scale roughness features caused by the SiC abrasive paper (Figure 3b). The bare Al curve shows active corrosion upon anodic polarization; this is due to pitting corrosion with pits uniformly distributed over the entire surface (Figure 3c).⁶⁰ The substrate covered with the LISS coating shows a lower current density in the cathodic branch due to the lower conductivity of the PDMS-covered surface. However, during anodic polarization, active dissolution is still observed, with only slightly reduced anodic current densities

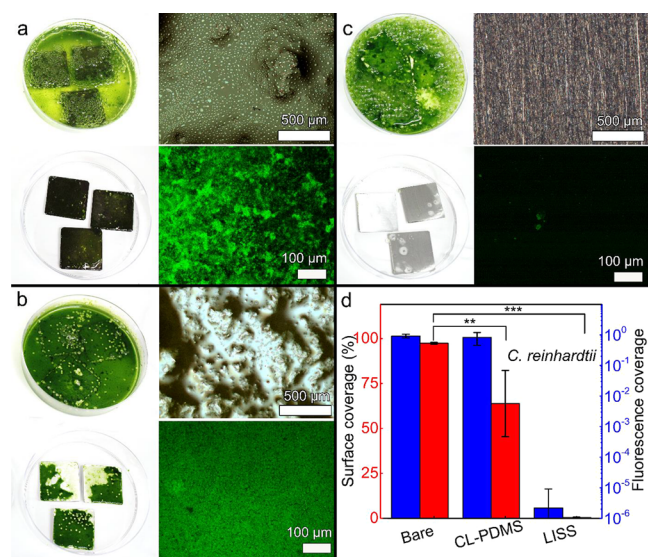


Figure 4. Digital images of aluminum samples immersed for 8 days in freshwater medium containing *C. reinhardtii* green algae just before (top-left) and immediately after (bottom-left) harvesting by passing through the water–air interface and corresponding bright-field reflectance (top-right) and fluorescence (bottom-right) images obtained immediately after harvesting. (a) Bare, (b) CL-PDMS, and (c) LISS. (d) Calculated surface coverage as obtained from digital (red columns) and fluorescence (blue columns) images. Note that fluorescence coverage is plotted on a logarithmic scale.

surfaces covering $97.4 \pm 0.5\%$ of the total sample area (Figure 4a,d and Movie S1, Supporting Information). Furthermore, all bare Al samples showed severe corrosion, resulting in the appearance of dark green-black color (Figure 4a). The biofilms formed on the CL-PDMS samples covered $63.8 \pm 18.4\%$ of the total sample area without showing any signs of corrosion (Figure 4b,d and Movie S2, Supporting Information). When the Petri dish containing LISS Al samples was immersed in a larger reservoir of fresh water prior to harvesting, the algal biofilm spontaneously delaminated from the LISS substrates. When pulled through the water–air interface, $99.6 \pm 0.3\%$ of the Al surface was both biofilm-free and corrosion-free, showing a highly reflective metallic luster (Figure 4c,d and Movie S3, Supporting Information). Statistical analysis was performed to determine the significance of the resistance of the coated samples to freshwater green algae and showed a p -value of 0.045 and $\ll 0.005$ for CL-PDMS and LISS aluminum, respectively (Figure 4d).

Although bacteria are usually associated with primary biofilm communities, other microscopic organisms such as diatoms are also known to be early colonizers.^{38,39} Diatoms are unicellular algae, in which the protoplast is enclosed in an elaborately decorated silica shell (the frustule) composed of overlapping halves or “valves”.⁶⁵ Diatoms adhere to surfaces through the production of sticky extracellular polymeric substances, which are secreted through an elongated slit in one or both valves, while the division of attached cells rapidly gives rise to colonies that eventually coalesce to form a compact biofilm.^{36,66} While silicone elastomers have been investigated and commercially tested with anti-biofouling paints to “release” fouling organisms under hydrodynamic conditions,³⁸ it has been demonstrated that diatoms can barely be released from PDMS elastomer coatings even under high-speed operating conditions (>30 knots).^{38,66} Therefore, it is critical to evaluate the developed

coatings for their fouling release characteristics against early colonizers. *Odontella aurita* is the benthic diatom that belongs to the cosmopolitan taxa category and can be found in the Arctic, sub-Arctic, and even in tropical marine waters.⁶⁷ It is an unicellular organism, a cylindrical, chain-forming diatom with a yellow to brown color. The cells are connected to each other by protrusions that extend from the end of each cell. *O. aurita* can either swim freely in the water or be firmly attached to rocks, plants, or animals. It has also been shown that *O. aurita* can act as a substrate for other diatoms in freshwater, brackish, and marine environments.⁶⁸

The treated and control samples were immersed in seawater growth media containing *O. aurita* diatoms for 8 days under a 16/8 h on/off lighting cycle, and the results are summarized in Figure 5. Again, there was a significant increase in diatom

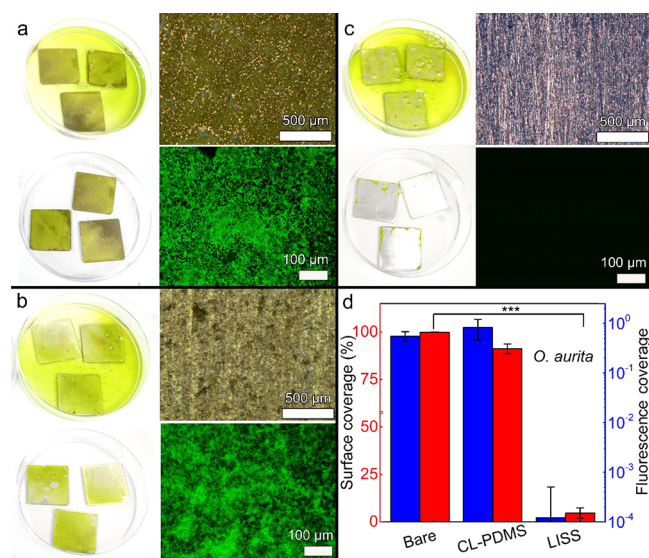


Figure 5. Digital images of aluminum samples immersed for 8 days in seawater medium with *O. aurita* diatoms just before (upper-left) and immediately after (lower-left) harvesting by passing through the water–air interface and corresponding bright-field reflectance (upper-right) and fluorescence (lower-right) images obtained immediately after the harvesting of (a) bare, (b) CL-PDMS, and (c) LISS. (d) Calculated surface coverage from digital (red columns) and fluorescence (blue columns) images. Note that fluorescence coverage is plotted on a logarithmic scale.

density in all samples over the growth period. Surface coverage calculations were performed using digital and confocal fluorescence microscopy images. Bare and CL-PDMS samples were pulled through a water–air interface and showed surface coverage of 99.9 ± 0.1 and $91.2 \pm 2.6\%$, respectively (Figure 5a,b,d and Movies S4 and S5, Supporting Information). The surface coverage of the LISS samples was $4.6 \pm 2.7\%$, a significant difference ($p \ll 0.005$) compared to the bare and CL-PDMS samples (Figure 5c,d and Movie S6, Supporting Information). Such passive shedding, i.e., no external stimuli applied to remove the biofilm rather than pulling it through a water–air interface, indicates poor adhesion of the diatom biofilms to the LISS-coated Al substrates. Furthermore, all treated substrates, i.e., CL-PDMS and LISS, exhibit a well-reflective metallic luster after 8 days of immersion in seawater media, indicating superior resistance to a highly corrosive environment (Figure 5b,c).

4. CONCLUSIONS

In this study, we further explored a one-pot approach of UV-grafting of PDMS to convert a surface of Al into LISS. Here, PDMS was covalently grafted to Al by UV irradiation at a specific wavelength and served as a surface energy-reducing agent, while the remaining unbound oil was simultaneously utilized as an infusing lubricant. Our approach does not require harsh pre/post-grafting treatments or micro- or hierarchical micro/nano-surface structuring to be suitable for industrial applications, making it advantageous over superhydrophobic and SLIPS surfaces as long as the substrate is UV-stable, i.e., metals, metal oxides, ceramics, and glasses. Since Al is used in highly corrosive environments and at the same time is susceptible to biofouling, the UV-grafted Al samples were investigated for their corrosion resistance in aqueous environments with and without aquatic organisms such as freshwater algae and seawater diatoms. We investigated two types of coatings: (i) semi-rigid, CL-PDMS and (ii) liquid-like LISS, which were obtained by different exposure times to UV irradiation. While bare Al corroded severely in seawater media within a short period of exposure, both coatings exhibited superior corrosion resistance, showing a corrosion-free surface after 143 days of immersion. The latter was also confirmed by potentiodynamic polarization measurements, especially for the CL-PDMS coating. This superior corrosion resistance was attributed to the inability of the corrosive electrolyte to penetrate the CL-PDMS layer, which was also firmly attached to the Al substrate. To test the biofouling resistance of the UV-grafted coatings, the bare and coated Al surfaces were exposed for 8 days to a medium containing aquatic species such as freshwater *C. reinhardtii* algae and seawater *O. aurita* diatoms. While both coatings exhibited superior corrosion resistance, LISS prevented almost complete biofilm attachment of both aquatic species in short-term laboratory studies. In contrast to CL-PDMS, the presence of residual, unbound silicone oil in LISS enhances the anti-biofouling performance of PDMS by forming an additional stable liquid–liquid interface that separates the solid surface from the fouling liquid media.⁶⁹ Despite the superior corrosion resistance, the CL-PDMS coating should be further investigated for its damage tolerance, while the self-healing properties imparted to CL-PDMS by the infusions of silicone oil could further improve the overall corrosion resistance. Given the above advantages and considering that the proposed approach is easy to implement, fast, nontoxic, environmentally friendly, scalable, and inexpensive, we envision that the UV-grafting approach of PDMS will advance the development of a nontoxic omni-repellent and corrosion-resistant coating technology for challenging but highly desirable aquatic applications.

■ ASSOCIATED CONTENT

SI Supporting Information

The Supporting Information is available free of charge at <https://pubs.acs.org/doi/10.1021/acsami.3c04508>.

Typical UV–vis spectrum of a medium-pressure mercury UV lamp; high-resolution XPS C 1s spectrum measured on polished Al substrates; typical XPS survey spectrum of UV-grafted PDMS on Al and bare Al substrates; high-resolution O 1s XPS spectra of UV-grafted PDMS on Al substrates measured at 75° angle; angle-resolved high-resolution Al 2p XPS spectra of UV-grafted PDMS on Al substrates; SEM images of the

cross-linked silicone oil on Al foil; corrosion of LISS-coated Al on edges; time-lapse digital and bright-field optical microscopy images of Al samples in freshwater and seawater media after 85 and 143 days of exposure; chemical composition of freshwater medium; and chemical composition of seawater medium (PDF)

Movie S1. Shading of the green algal biofilm from bare Al substrate surfaces during the transition through a water–air interface (MP4)

Movie S2. Green algal biofilm shadowing on CL-PDMS Al substrate surfaces during the transition through a water–air interface (MP4)

Movie S3. Green algae biofilm shadowing on LISS Al substrate surfaces during the transition through a water–air interface (MP4)

Movie S4. Diatom biofilm shading of bare Al substrate surfaces during the transition through a water–air interface (MP4)

Movie S5. Diatom biofilm shading on CL-PDMS Al substrate surfaces during the transition through a water–air interface (MP4)

Movie S6. Diatom biofilm shading of LISS Al substrate surfaces during the transition through a water–air interface (MP4)

■ AUTHOR INFORMATION

Corresponding Authors

Wolfgang H. Goldmann – Department of Physics, Biophysics Group, Friedrich-Alexander-Universität Erlangen-Nürnberg, Erlangen 91052, Germany; Email: wolfgang.goldmann@fau.de

Alexander B. Tesler – Department of Materials Science and Engineering, Institute for Surface Science and Corrosion, Faculty of Engineering, Friedrich-Alexander-Universität Erlangen-Nürnberg, Erlangen 91058, Germany; orcid.org/0000-0003-3425-7667; Email: alexander.tesler@fau.de

Authors

Lucia H. Prado – Department of Materials Science and Engineering, Institute for Surface Science and Corrosion, Faculty of Engineering, Friedrich-Alexander-Universität Erlangen-Nürnberg, Erlangen 91058, Germany; orcid.org/0000-0002-6311-5601

David Böhringer – Department of Physics, Biophysics Group, Friedrich-Alexander-Universität Erlangen-Nürnberg, Erlangen 91052, Germany

Anca Mazare – Department of Materials Science and Engineering, Institute for Surface Science and Corrosion, Faculty of Engineering, Friedrich-Alexander-Universität Erlangen-Nürnberg, Erlangen 91058, Germany

Lamborghini Sotelo – Institute for Nanotechnology and Correlative Microscopy eV INAM, Fraunhofer Institute, Forchheim 91301, Germany; Department of Physics, Institute for Optics, Information and Photonics, Friedrich-Alexander-Universität Erlangen-Nürnberg, Erlangen 91058, Germany

George Sarau – Institute for Nanotechnology and Correlative Microscopy eV INAM, Fraunhofer Institute, Forchheim 91301, Germany; Fraunhofer Institute for Ceramic Technologies and Systems IKTS, Forchheim 91301, Germany; Max Planck Institute for the Science of Light, Erlangen 91058, Germany

Silke Christiansen – Institute for Nanotechnology and Correlative Microscopy eV INAM, Fraunhofer Institute, Forchheim 91301, Germany; Fraunhofer Institute for Ceramic Technologies and Systems IKTS, Forchheim 91301, Germany; Institute for Experimental Physics, Freie Universität Berlin, Berlin 14195, Germany; orcid.org/0000-0002-4908-4087

Ben Fabry – Department of Physics, Biophysics Group, Friedrich-Alexander-Universität Erlangen-Nürnberg, Erlangen 91052, Germany

Patrik Schmuki – Department of Materials Science and Engineering, Institute for Surface Science and Corrosion, Faculty of Engineering, Friedrich-Alexander-Universität Erlangen-Nürnberg, Erlangen 91058, Germany; Regional Centre of Advanced Technologies and Materials, Palacky University, Olomouc 772 07, Czech Republic; orcid.org/0000-0002-9208-5771

Sannakaisa Virtanen – Department of Materials Science and Engineering, Institute for Surface Science and Corrosion, Faculty of Engineering, Friedrich-Alexander-Universität Erlangen-Nürnberg, Erlangen 91058, Germany

Complete contact information is available at:
<https://pubs.acs.org/10.1021/acsami.3c04508>

Author Contributions

L.H.P. carried out laboratory research on the preparation and coating of the samples and corrosion experiments, D.B. carried out algal and diatom biofilm characterization, A.M. carried out XPS measurements, L.S. carried out Raman measurements, G.S. carried out and analyzed Raman measurements, S.C. supervised Raman measurements, B.F. conceptualized and supervised biofouling experiments, P.S. conceptualized experiments, S.V. conceptualized and supervised corrosion experiments, W.H.G. conceptualized and supervised biofouling experiments, A.B.T. conceptualized experiments and carried out laboratory research on the preparation and coating of the samples, wetting, FTIR measurements, and biofouling experiments. The manuscript was written and completed with the contributions of all authors. All authors approved the final version of the manuscript.

Notes

The authors declare no competing financial interest.

ACKNOWLEDGMENTS

The authors thank the DFG and the DFG Cluster of Excellence EAM for financial support. A.B.T. and W.H.G. thank the DFG (grant number 442826449; SCHM 1597/38-1 and FA 336/13-1) for financial support. The authors thank the Nürnberg Zoo for providing the recipe and materials for the preparation of the artificial seawater medium. L.S. and S.C. were supported by the European Union's H2020 research and innovation program under the Marie Skłodowska-Curie grant agreement AIMed no. 861138, 2020-2023. G.S. and S.C. acknowledge the financial support from the European Union within the research projects 4D + nanoSCOPE, LRI C10, and by the "Freistaat Bayern" and European Union within the project Analytiktechnikum für Gesundheits- und Umweltforschung AGEUM, StMWi-43-6623-22/1/3. The authors thank Ms. Helga Hildebrand for the XPS measurements.

REFERENCES

- (1) Uihlein, A.; Magagna, D. Wave and Tidal Current Energy – a Review of the Current State of Research Beyond Technology. *Renewable Sustainable Energy Rev.* **2016**, *58*, 1070–1081.
- (2) Martínez, M. L.; Silva, R.; Garcia, J. How Can We Use Ocean Energy to Generate Electricity? *Front. Young Minds* **2021**, *9*, No. 609510.
- (3) Melikoglu, M. Current Status and Future of Ocean Energy Sources: A Global Review. *Ocean Eng.* **2018**, *148*, 563–573.
- (4) Freeman, S.; Green, J. In *Aluminum in the Marine Environment: An Update*, OCEANS 2000 MTS/IEEE Conference and Exhibition. Conference Proceedings (Cat. No.00CH37158), Providence, RI, USA, 11–14 September; IEEE: Providence, RI, USA, 2000; vol.3, pp 1591–1595.
- (5) Pfeiffer, O. P.; Liu, H.; Montanelli, L.; Latypov, M. I.; Sen, F. G.; Hegadekatte, V.; Olivetti, E. A.; Homer, E. R. Aluminum Alloy Compositions and Properties Extracted from a Corpus of Scientific Manuscripts and Us Patents. *Sci. Data* **2022**, *9*, 128.
- (6) Georgantzia, E.; Gkantou, M.; Kamaris, G. S. Aluminium Alloys as Structural Material: A Review of Research. *Eng. Struct.* **2021**, *227*, No. 111372.
- (7) Ghali, E., Active and Passive Behaviors of Aluminum and Magnesium and Their Alloys. In *Corrosion Resistance of Aluminum and Magnesium Alloys*, 2010; pp 78–120.
- (8) Vedder, W.; Vermilyea, D. A. Aluminum + Water Reaction. *Trans. Faraday Soc.* **1969**, *65*, 561–584.
- (9) Alwitt, R. S. The Growth of Hydrous Oxide Films on Aluminum. *J. Electrochem. Soc.* **1974**, *121*, 1322.
- (10) Szklarska-Smialowska, Z. Pitting Corrosion of Aluminum. *Corros. Sci.* **1999**, *41*, 1743–1767.
- (11) Sparling, D. W.; Lowe, T. P., Environmental Hazards of Aluminum to Plants, Invertebrates, Fish, and Wildlife. In *Reviews of Environmental Contamination and Toxicology*; Ware, G. W.; Gunther, F. A., Eds.; Springer New York: New York, NY, 1996; pp. 1–127.
- (12) Exley, C., Aluminum in Biological Systems. In *Encyclopedia of Metalloproteins*; Kretsinger, R. H.; Uversky, V. N.; Permyakov, E. A., Eds.; Springer New York: New York, NY, 2013; pp 33–34.
- (13) Gensemer, R. W.; Playle, R. C. The Bioavailability and Toxicity of Aluminum in Aquatic Environments. *Crit. Rev. Environ. Sci. Technol.* **1999**, *29*, 315–450.
- (14) Bixler, G. D.; Bhushan, B. Biofouling: Lessons from Nature. *Philos. Trans. R. Soc., A* **2012**, *370*, 2381–2417.
- (15) Railkin, A. I., *Marine Biofouling: Colonization Processes and Defenses*; CRC Press INC.: Boca Raton, 2003; p 320.
- (16) Woods Hole Oceanographic Institution. Chapter 11: The History of the Prevention of Fouling. In *Marine fouling and its prevention; prepared for Bureau of Ships, Navy Dept.*; George Banta Publishing Company: Menasha, Wisconsin, 1952; p 388.
- (17) Yebra, D. M.; Kiil, S.; Dam-Johansen, K. Antifouling Technology—Past, Present and Future Steps Towards Efficient and Environmentally Friendly Antifouling Coatings. *Prog. Org. Coat.* **2004**, *50*, 75–104.
- (18) Buskens, P.; Wouters, M.; Rentrop, C.; Vroon, Z. A Brief Review of Environmentally Benign Antifouling and Foul-Release Coatings for Marine Applications. *J. Coat. Technol. Res.* **2013**, *10*, 29–36.
- (19) Pei, X.; Ye, Q., Development of Marine Antifouling Coatings. In *Antifouling Surfaces and Materials: From Land to Marine Environment*; Zhou, F., Ed.; Springer Berlin Heidelberg: Berlin, Heidelberg, 2015; pp 135–149.
- (20) Lejars, M.; Margaillan, A.; Bressy, C. Fouling Release Coatings: A Nontoxic Alternative to Biocidal Antifouling Coatings. *Chem. Rev.* **2012**, *112*, 4347–4390.
- (21) Genzer, J.; Efimenko, K. Recent Developments in Superhydrophobic Surfaces and Their Relevance to Marine Fouling: A Review. *Biofouling* **2006**, *22*, 339–360.
- (22) Hwang, G. B.; Page, K.; Patir, A.; Nair, S. P.; Allan, E.; Parkin, I. P. The Anti-Biofouling Properties of Superhydrophobic Surfaces Are Short-Lived. *ACS Nano* **2018**, *12*, 6050–6058.

- (23) Wong, T.-S.; Kang, S. H.; Tang, S. K. Y.; Smythe, E. J.; Hatton, B. D.; Grinthal, A.; Aizenberg, J. Bioinspired Self-Repairing Slippery Surfaces with Pressure-Stable Omniphobicity. *Nature* **2011**, *477*, 443–447.
- (24) Tesler, A. B.; Kim, P.; Kolle, S.; Howell, C.; Ahanotu, O.; Aizenberg, J. Extremely Durable Biofouling-Resistant Metallic Surfaces Based on Electrodeposited Nanoporous Tungstite Films on Steel. *Nat. Commun.* **2015**, *6*, 8649.
- (25) Deng, R.; Shen, T.; Chen, H.; Lu, J.; Yang, H.-C.; Li, W. Slippery Liquid-Infused Porous Surfaces (Slipss): A Perfect Solution to Both Marine Fouling and Corrosion? *J. Mater. Chem. A* **2020**, *8*, 7536–7547.
- (26) Yao, W.; Wu, L.; Sun, L.; Jiang, B.; Pan, F. Recent Developments in Slippery Liquid-Infused Porous Surface. *Prog. Org. Coat.* **2022**, *166*, No. 106806.
- (27) Huang, C.; Guo, Z. Fabrications and Applications of Slippery Liquid-Infused Porous Surfaces Inspired from Nature: A Review. *J. Bionic Eng.* **2019**, *16*, 769–793.
- (28) Villegas, M.; Zhang, Y.; Abu Jarad, N.; Soleymani, L.; Didar, T. F. Liquid-Infused Surfaces: A Review of Theory, Design, and Applications. *ACS Nano* **2019**, *13*, 8517–8536.
- (29) Yang, X.; Huang, Y.; Zhao, Y.; Zhang, X.; Wang, J.; Sann, E. E.; Mon, K. H.; Lou, X.; Xia, F. Bioinspired Slippery Lubricant-Infused Surfaces with External Stimuli Responsive Wettability: A Mini Review. *Front. Chem.* **2019**, *7*, 826.
- (30) Zhang, Y.; Han, Y.; Ji, X.; Zang, D.; Qiao, L.; Sheng, Z.; Wang, C.; Wang, S.; Wang, M.; Hou, Y.; Chen, X.; Hou, X. Continuous Air Purification by Aqueous Interface Filtration and Absorption. *Nature* **2022**, *610*, 74–80.
- (31) Zhang, Y.; Hou, X. Liquid-Based Materials. *Natl. Sci. Open* **2022**, *1*, No. 20220035.
- (32) Liu, J.; Xu, X.; Lei, Y.; Zhang, M.; Sheng, Z.; Wang, H.; Cao, M.; Zhang, J.; Hou, X. Liquid Gating Meniscus-Shaped Deformable Magnetoelastic Membranes with Self-Driven Regulation of Gas/Liquid Release. *Adv. Mater.* **2022**, *34*, No. 2107327.
- (33) Chen, B.; Zhang, R.; Hou, Y.; Zhang, J.; Chen, S.; Han, Y.; Chen, X.; Hou, X. Light-Responsive and Corrosion-Resistant Gas Valve with Non-Thermal Effective Liquid-Gating Positional Flow Control. *Light: Sci. Appl.* **2021**, *10*, 127.
- (34) Lee, J.; Lee, M.-H.; Choi, C.-H. Design of Robust Lubricant-Infused Surfaces for Anti-Corrosion. *ACS Appl. Mater. Interfaces* **2022**, *14*, 2411–2423.
- (35) Tesler, A. B.; Prado, L. H.; Khusniyarov, M.; Thievensen, I.; Mazare, A.; Fischer, L.; Virtanen, S.; Goldmann, W. H.; Schmuki, P. A One-Pot Universal Approach to Fabricate Lubricant-Infused Slippery Surfaces on Solid Substrates. *Adv. Funct. Mater.* **2021**, *31*, No. 2101090.
- (36) Tesler, A. B.; Prado, L. H.; Thievensen, I.; Mazare, A.; Schmuki, P.; Virtanen, S.; Goldmann, W. H. Nontoxic Liquid-Infused Slippery Coating Prepared on Steel Substrates Inhibits Corrosion and Biofouling Adhesion. *ACS Appl. Mater. Interfaces* **2022**, *14*, 29386–29397.
- (37) Trasatti, S., Electrochemical Theory | Oxygen Evolution. In *Encyclopedia of Electrochemical Power Sources*; Garce, J., Ed.; Elsevier: Amsterdam, 2009; pp 49–55, DOI: 10.1016/B978-0-444-52745-5.00023-X.
- (38) Hu, P.; Xie, Q.; Ma, C.; Zhang, G. Silicone-Based Fouling-Release Coatings for Marine Antifouling. *Langmuir* **2020**, *36*, 2170–2183.
- (39) Robinson, N. J.; Majewska, R.; Lazo-Wasem, E. A.; Nel, R.; Paladino, F. V.; Rojas, L.; Zardus, J. D.; Pinou, T. Epibiotic Diatoms Are Universally Present on All Sea Turtle Species. *PLoS One* **2016**, *11*, No. e0157011.
- (40) Baensch, H. A.; Debelius, H., *Meerwasser Atlas 1: Die Gemeinsame Pflege Von Wirbellosen Tieren Und Tropischen Meeresfischen Im Aquarium*; Mergus-Verlag GmbH: Osnabrück, 2006.
- (41) Forrest, E.; Schulze, R.; Liu, C.; Dombrowski, D. Influence of Surface Contamination on the Wettability of Heat Transfer Surfaces. *Int. J. Heat Mass Transfer* **2015**, *91*, 311–317.
- (42) Rahimi, M.; Afshari, A.; Thormann, E. Effect of Aluminum Substrate Surface Modification on Wettability and Freezing Delay of Water Droplet at Subzero Temperatures. *ACS Appl. Mater. Interfaces* **2016**, *8*, 11147–11153.
- (43) Greczynski, G.; Hultman, L. Undressing the Myth of Apparent Constant Binding Energy of the C 1S Peak from Adventitious Carbon in X-Ray Photoelectron Spectroscopy. *Sci. Talks* **2022**, *1*, No. 100007.
- (44) Tesler, A. B.; Sheng, Z.; Lv, W.; Fan, Y.; Fricke, D.; Park, K.-C.; Alvarenga, J.; Aizenberg, J.; Hou, X. Metallic Liquid Gating Membranes. *ACS Nano* **2020**, *14*, 2465–2474.
- (45) Kaur, A.; Chahal, P.; Hogan, T. Selective Fabrication of Sic/Si Diodes by Excimer Laser under Ambient Conditions. *IEEE Electron Device Lett.* **2016**, *37*, 142–145.
- (46) Pertsin, A. J.; Gorelova, M. M.; Levin, V. Y.; Makarova, L. I. An Xps Study of the Surface–Bulk Compositional Differences in Siloxane-Containing Block Copolymers and Polymer Blends. *J. Appl. Polym. Sci.* **1992**, *45*, 1195–1202.
- (47) Wooh, S.; Encinas, N.; Vollmer, D.; Butt, H.-J. Stable Hydrophobic Metal-Oxide Photocatalysts Via Grafting Polydimethylsiloxane Brush. *Adv. Mater.* **2017**, *29*, No. 1604637.
- (48) Crist, B. V., *Handbook of Monochromatic Xps Spectra: The Elements of Native Oxides*; Wiley, 2000.
- (49) Moulder, J. F.; Stickle, W. F.; Sobol, W. M.; Bomben, K. D. In *Handbook of X-Ray Photoelectron Spectroscopy*, 1992.
- (50) Greczynski, G.; Hultman, L. The Same Chemical State of Carbon Gives Rise to Two Peaks in X-Ray Photoelectron Spectroscopy. *Sci. Rep.* **2021**, *11*, 11195.
- (51) Sabata, A.; van Ooij, W. J.; Yasuda, H. K. Plasma-Polymerized Films of Trimethylsilane Deposited on Cold-Rolled Steel Substrates. Part I. Characterization by Xps, Aes and Tof-Sims. *Surf. Interface Anal.* **1993**, *20*, 845–859.
- (52) Bao, C.; Xu, K.-Q.; Tang, C.-Y.; Lau, W.-M.; Yin, C.-B.; Zhu, Y.; Mei, J.; Lee, J.; Hui, D.; Nie, H.-Y.; Liu, Y. Cross-Linking the Surface of Cured Polydimethylsiloxane Via Hyperthermal Hydrogen Projectile Bombardment. *ACS Appl. Mater. Interfaces* **2015**, *7*, 8515–8524.
- (53) Damayanti, N. P. Preparation of Superhydrophobic Pet Fabric from Al₂O₃–SiO₂ Hybrid: Geometrical Approach to Create High Contact Angle Surface from Low Contact Angle Materials. *J. Sol-Gel Sci. Technol.* **2010**, *56*, 47–52.
- (54) Pemberger, N.; Bittner, L.; Huck, C. Using near-Infrared Spectroscopy to Monitor the Curing Reaction of Silicone Adhesives. *Spectroscopy* **2015**, *30*, 8.
- (55) Snyder, R. G.; Strauss, H. L.; Elliger, C. A. Carbon-Hydrogen Stretching Modes and the Structure of N-Alkyl Chains. 1. Long, Disordered Chains. *J. Phys. Chem.* **1982**, *86*, 5145–5150.
- (56) Ron, H.; Cohen, H.; Matlis, S.; Rappaport, M.; Rubinstein, I. Self-Assembled Monolayers on Oxidized Metals. 4. Superior N-Alkanethiol Monolayers on Copper. *J. Phys. Chem. B* **1998**, *102*, 9861–9869.
- (57) Bae, S. C.; Lee, H.; Lin, Z.; Granick, S. Chemical Imaging in a Surface Forces Apparatus: Confocal Raman Spectroscopy of Confined Poly(Dimethylsiloxane). *Langmuir* **2005**, *21*, 5685–5688.
- (58) Alshehri, A. M.; Deepak, K. L. N.; Marquez, D. T.; Desgreniers, S.; Bhardwaj, V. R. Localized Nanoclusters Formation in Pdms Upon Irradiation with Femtosecond Laser. *Opt. Mater. Express* **2015**, *5*, 858–869.
- (59) Venkatachalam, S.; Hourlier, D. Heat Treatment of Commercial Polydimethylsiloxane Pdms Precursors: Part I. Towards Conversion of Patternable Soft Gels into Hard Ceramics. *Ceram. Int.* **2019**, *45*, 6255–6262.
- (60) Vargel, C., Types of Corrosion on Aluminium. In *Corrosion of Aluminium*; Vargel, C., Ed.; Elsevier: Amsterdam, 2004; pp 113–146.
- (61) Wong, W. S. Y.; Hauer, L.; Naga, A.; Kaltbeitzel, A.; Baumli, P.; Berger, R.; D’Acunzi, M.; Vollmer, D.; Butt, H.-J. Adaptive Wetting of Polydimethylsiloxane. *Langmuir* **2020**, *36*, 7236–7245.
- (62) Callow, J. A.; Callow, M. E., Biofilms. In *Antifouling Compounds*; Fusetani, N.; Clare, A. S., Eds.; Springer Berlin

Heidelberg: Berlin, Heidelberg, 2006; pp 141–169, DOI: [10.1007/3-540-30016-3_6](https://doi.org/10.1007/3-540-30016-3_6).

(63) Paink, G. K.; Kolle, S.; Le, D.; Weaver, J. C.; Alvarenga, J.; Ahanotu, O.; Aizenberg, J.; Kim, P. Dynamic Self-Repairing Hybrid Liquid-in-Solid Protective Barrier for Cementitious Materials. *ACS Appl. Mater. Interfaces* **2020**, *12*, 31922–31932.

(64) Howell, C.; Vu, T. L.; Lin, J. J.; Kolle, S.; Juthani, N.; Watson, E.; Weaver, J. C.; Alvarenga, J.; Aizenberg, J. Self-Replenishing Vascularized Fouling-Release Surfaces. *ACS Appl. Mater. Interfaces* **2014**, *6*, 13299–13307.

(65) Chiovitti, A.; Dugdale, T. M.; Wetherbee, R., Diatom Adhesives: Molecular and Mechanical Properties. In *Biological Adhesives*; Smith, A. M.; Callow, J. A., Eds.; Springer Berlin Heidelberg: Berlin, Heidelberg, 2006; pp 79–103.

(66) Holland, R.; Dugdale, T. M.; Wetherbee, R.; Brennan, A. B.; Finlay, J. A.; Callow, J. A.; Callow, M. E. Adhesion and Motility of Fouling Diatoms on a Silicone Elastomer. *Biofouling* **2004**, *20*, 323–329.

(67) Witon, E.; Witkowski, A. Holocene Diatoms (Bacillariophyceae) from Faeroe Islands Fjords, Northern Atlantic Ocean. II. Distribution and Taxonomy of Marine Taxa with Special Reference to Benthic Forms. *Diatom Res.* **2006**, *21*, 175–215.

(68) Tiffany, M. A.; Lange, C. B. Diatoms Provide Attachment Sites for Other Diatoms: A Natural History of Epiphytism from Southern California. *Phycologia* **2002**, *41*, 116–124.

(69) Kolle, S.; Ahanotu, O.; Meeks, A.; Stafslie, S.; Kreder, M.; Vanderwal, L.; Cohen, L.; Waltz, G.; Lim, C. S.; Slocum, D.; Maldonado-Greene, E.; Hunsucker, K.; Swain, G.; Wendt, D.; Lay-Ming Teo, S.; Aizenberg, J. On the Mechanism of Marine Fouling-Prevention Performance of Oil-Containing Silicone Elastomers. *Sci. Rep.* **2022**, *12*, 11799.